Self-assembly of a Triblock Copolymer in the Presence of a Rigid Conjugated Polyelectrolyte

Karen Li[a], *Kiran Vaddi*[a], *Soenke Seifert*[b], *Jitendra Mata*[c,d], *Lilo D Pozzo*[a]*

[a]Department of Chemical Engineering, University of Washington, Seattle, WA, 98195, USA

[b]Advanced Photon Source (APS), Argonne National Laboratory (ANL), Lemont, IL, 60439, USA

[c]Australian Centre for Neutron Scattering (ACNS), Australian Nuclear Science and Technology Organisation (ANSTO), Lucas Heights, NSW 2234, Australia

[d]School of Chemistry, University of New South Wales, Sydney, NSW 2052, Australia

*Corresponding Author Email: dpozzo@uw.edu

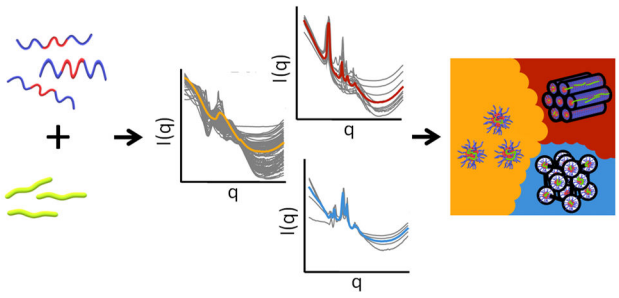

For Table of Contents use only

Abstract

The properties of conducting polymers are strongly influenced by structural changes induced by long-range order, which can be achieved using block copolymers that self-assemble into crystalline structures. These blends result in unique mesophases distinct from the pure components, with self-assembly behavior modulated by solution conditions and polymer architectures. High-throughput small angle x-ray scattering data of aqueous Pluronic P123 (PEO_{20}-PPO_{70}-PEO_{20}) and conjugated polyelectrolyte poly[3-(potassium-4-butanoate) thiophene-2,5-diyl] (PPBT) blends at various concentrations and temperatures were automatically classified into phase maps by *autophasemap*, an unsupervised statistical analysis algorithm. The outlined phase boundaries revealed that adding PPBT to high P123 concentrations induced a transition from cubic-ordered spherical micelles to hexagonally packed cylindrical micelles. Shear alignment via rheological small angle neutron scattering of the blends produced monolithic oriented cubic and hexagonal crystal gels. These insights into the self-assembly of conductive polymer blends will aid in the design of soft materials with tunable structural and electronic properties.

Introduction

Conjugated polymers (CPs) are commonly found in the active layers of organic electronic devices including photovoltaics (OPVs), electrochemical transistors (OECTs), bioelectronics, flexible devices, and more[1–6]. The electronic conduction of CPs is due to their π-conjugated structure, resulting in weakly bound electrons that can travel intra-chain through delocalized π-orbitals along the polymer backbone and inter-chain if there is sufficient π–π overlap. The conjugated structure typically makes these polymers more rigid than conventional polymers due to the loss of torsional rotation along sp^3 hybridized σ bonds and bond bending[7]. This is especially

important for the conductive properties of CPs as chain rigidity governs electronic properties including intrachain charge transport and interchain electronic coupling[8,9]. While conjugated polymers offer valuable electronic capabilities, they can be environmentally sensitive and brittle. These concerns can be addressed by formulating polymer blends, such as combining CPs with commodity polymers (e.g. polystyrene), to increase the mechanical robustness of the conductive material without severely impacting electronic properties[10,11]. Blending components to modify compositions of composite conjugated soft materials also avoid synthesizing complex macromolecules with the aim of achieving all the desired properties in a single material component. This can greatly simplify and accelerate the molecular design process to achieve material solutions via careful (re)-formulation instead of synthesis.

Block copolymers (BCPs) are commonly used templating materials for nanoparticles to create highly ordered nanostructures and have been demonstrated to lead to desirable characteristics including mechanical durability, long-range organization, and ionic conductivity[12–14]. Amphiphilic BCPs, composed of distinct hydrophilic and hydrophobic polymer blocks covalently bonded into a common chain, show rich self-assembling behavior in solid-states and in solution[15]. In dilute conditions, BCPs will usually form spherical or cylindrical micelles governed by thermodynamics[16]. In concentrated solutions and melts, BCPs frequently self-assemble into soft crystals structures, including cubic, hexagonal cylinders, bicontinuous (e.g. gyroid), and lamellar geometries[12,17]. Crystalline phases can persist but can also be altered by the presence of additives, suggesting that structures and properties of composites can be tuned through careful control over interactions of the components in a composite blend[18,19]. In particular, conductive polymer composites with continuous phases have shown to have greater electronic and ionic conductivities[20–22].

In this study, we analyze blends of Pluronic P123 and Poly[3-(potassium-4-butanoate)thiophene-2,5-diyl] (PPBT). Pluronics are amphiphilic triblock copolymers with a center polypropylene oxide (PPO) segment and two identical polyethylene oxide (PEO) end-segments (PEO_x -PPO_y -PEO_z). Pluronics self-assemble into various crystal lattices in aqueous conditions coinciding with the gelation of the system to form a Pluronic hydrogel. This behavior has been extensively studied through rheology and scattering techniques[18,23,24]. Pluronic P123 (PEO_{20}-PPO_{70}-PEO_{20}) is known to form isotropic micelles, face centered cubic (FCC), hexagonal closed packed (HCP), hexagonal cylinders (HEX), and lamellar (LAM) phases depending on the temperature and the polymer concentrations in water[25,26]. P123 micelle diameters were reported to range approximately between 15 to 25 nm for samples at approximately 30 wt% in water[17,27,28]. Pluronics are also capable of alignment into monolithic single crystalline structures through the use of shear. Micelles in these colloidal crystals are connected by weak intermolecular interactions that are typically dominated by steric repulsion. Consequently, when shear is applied, micelles within a hydrogel can flow past one another making it possible to obtain a colloidal crystal in which most of the particles are part of the same crystal lattice and with the same orientation[19,29].

Poly[3-(potassium-4-butanoate)thiophene-2,5-diyl] (PPBT) is an anionic water-soluble conjugated polyelectrolyte that has been studies as a mixed ionic and electronic conductor and has been previously successfully aligned by nanocrystalline cellulose to a chiral nematic liquid crystal phase[30,31]. The primary objective of this work is to investigate the structural impact of formulating blends of Pluronic P123 and PPBT at variable concentrations and temperatures. We aim to outline how solution conditions (temperature, concentration, shear, etc.) and polymer architectures (molecular weight, side chains, etc.) affect the final morphology of a composite consisting of a

self-assembling non-conjugated block-polymer block copolymer (Pluronic P123) in the presence of a relatively rigid conjugated polyelectrolyte additive (PPBT) in aqueous solution.

Given the number of factors influencing the structure of complex polymer blends, high-throughput structural characterization is essential. This can be achieved through small-angle x-ray scattering (SAXS), a powerful technique that is highly compatible with laboratory automation, requires minimal sample, and is relatively accessible. SAXS provides insights into two key aspects of material structure. The form factor corresponds to the scattering from the size and shape of individual particles while the structure factor is related to the special correlation of the particles in the system. Thus, SAXS enables analysis of both particle morphology and collective ordering in complex materials. The SAXS data for Pluronics typically exhibits distinct, sharp Bragg's peaks when crystalline structures are present, facilitating precise phase identification. Thus, high-throughput SAXS (HT-SAXS) enables rapid capture of organized structures and phase transitions across a broad design space.

Moreover, we also aim to assess the potential for single-crystal mesophase formation in the composite blends though in-situ rheological small-angle neutron scattering (rheo-SANS), which allows us to observe shear-induced alignment. By combining HT-SAXS with rheo-SANS, this study offers a comprehensive view of the self-assembly and shear-alignment behavior of P123 and PPBT blends. These findings could contribute to the design of advanced conductive polymer systems with tunable structural and electrochemical properties for applications in energy storage[32], flexible electronics[33], and biosensors[34] amongst others.

Materials and Methods

Materials

Pluronic P123 (MW = 5.8 kg mol, PEO composition = 30wt%, Product 435465) was obtained from Sigma Aldrich (Burlington, MA). Two lots of PPBT (RR=89%, Product 4021), PTL37-92 (MW=13k/15 kg mol^{-1}, Pd=2.0) and PTL40-30 (MW=13k/16 kg mol^{-1}, Pd=2.2), were obtained from Rieke Metals (Lincoln, NE). All polymers were used without further purification or processing. H_2O was purified with a Millipore Direct Q system before use (electrical resistivity 18.2 MOhm cm). D_2O for in-situ rheo-SANS experiments was provided by the ANSTO OPAL facility during the beam time.

Polymer Blend Preparation

Samples were prepared with Pluronic P123 in methanol (10, 25, and 50 wt//v%) and aqueous PPBT stock solutions (1 and 5wt/v %) (Fig. 1a). These stock solutions were pipetted using an open-source liquid handling robot, Opentrons OT-2 (New York, NY), and dried at 60°C overnight (Fig. 1b). The remaining solids were dried under vacuum for 1 hour at room temperature to remove any remaining solvent. Water was then added to the dried polymers with the OT-2 to reach the desired concentration of PPBT (0-5 wt%) and Pluronic (5-40 wt%) in each sample.

Small Angle X-ray scattering (SAXS)

Structural characterization of the polymer blends was obtained through high-throughput small angle scattering (HT-SAXS). HT-SAXS measurements were taken at APS Beamline 12-ID-C. The instrument used an X-ray beam configuration of 21 keV, corresponding to a wavelength of 0.62 Å. The beam size was 0.4 mm x 0.15 mm, and the flux was approximately 2 x 10^{12} photons/s/mm^2. Samples with 25 wt% P123 or less were cooled to 7°C while sample with 30 wt% P123 or greater were cooled to -4°C to ensure all samples are fluid. The samples were loaded into custom-designed 10mm thick 48-sample cartridges[35] with Kapton windows. These cartridges were then cooled to -4°C to remove air bubbles from the samples before being mounted to the

instrument using an ambient temperature cartridge holder. These samples were measured at ambient temperature of 23℃. Temperature-controlled HT-SAXS experiments were also performed on a few select samples. Neat P123 samples (25-40 wt%) and blends (25-40 wt% P123 and 1wt % PPBT) were cooled to low temperatures again to become fluid before being loaded into thin-wall glass capillaries (80mm, 1.0mm O.D.). Samples were measured from 0 to 100℃ using a Peltier controller and were allowed to sit for 5 minutes in between each measurement to achieve temperature stabilization. Scattering profiles were radially integrated and normalized using a MATLAB series of routines that were developed and locally available at the beamline. The HT-SAXS data of the samples were then isolated by using empty Kapton cell or empty capillary background subtraction for the custom cartridge or capillary environment respectively (Fig. 1c).

A statistical analysis tool, *autophasemap*, developed by our group[36] and is capable of rapid analysis of spectral data from multiple techniques. The *autophasemap* algorithm was used to enable rapid analysis of phase maps based on scattering data from blend polymer formulations (Fig. 1d). This algorithm enables minimally supervised operation in two steps: identification and assignment. The identification step determines a set of template functions that best represent the observed features of the spectra. The samples are then assigned to templates by calculating a shape distance, which measures the similarity between the sample's profile and a template. The template functions undergo an iterative learning process, initiated by aligning each profile with the current templates and organizing them into groups based on the shape distance. In each iteration, the templates are subsequently updated to reflect the average of the aligned data within each group. *autophasemap* is available in in a GitHub repository, which can be accessed at https://github.com/pozzo-research-group/papers/tree/main/autophasemap[37]. We made a few changes related to stability and visualization of the algorithm presented in [36]: a) we perform the

initialization of templates using the approach presented in [38] and obtain a stable solution by performing the optimization of template identification and assignment over multiple runs (set to 20 unless otherwise specified); b) The phase map visualization also improved by using a Gaussian Process classifier trained using the approach presented in [39] on the composition and cluster labels as the training data. We observed that this approach allowed us to provide better interpolation of the discrete clustering labels observed on our sampled design space. Given that our sampling of design space is discrete, we used the Gaussian Process classifier to interpolate the labels on a regular grid of higher resolution (30 points along each dimension). This interpolation results in a probability to each point in the design space that measures the similarity to corresponding template. These points were then classified to a phase represented by a template if their probability met a minimum threshold. After automatic clustering of the data, crystalline phases of the polymer blends were classified as lyotropic liquid crystals through peak spacing ratios of Bragg peaks in the 1D SAXS profiles.

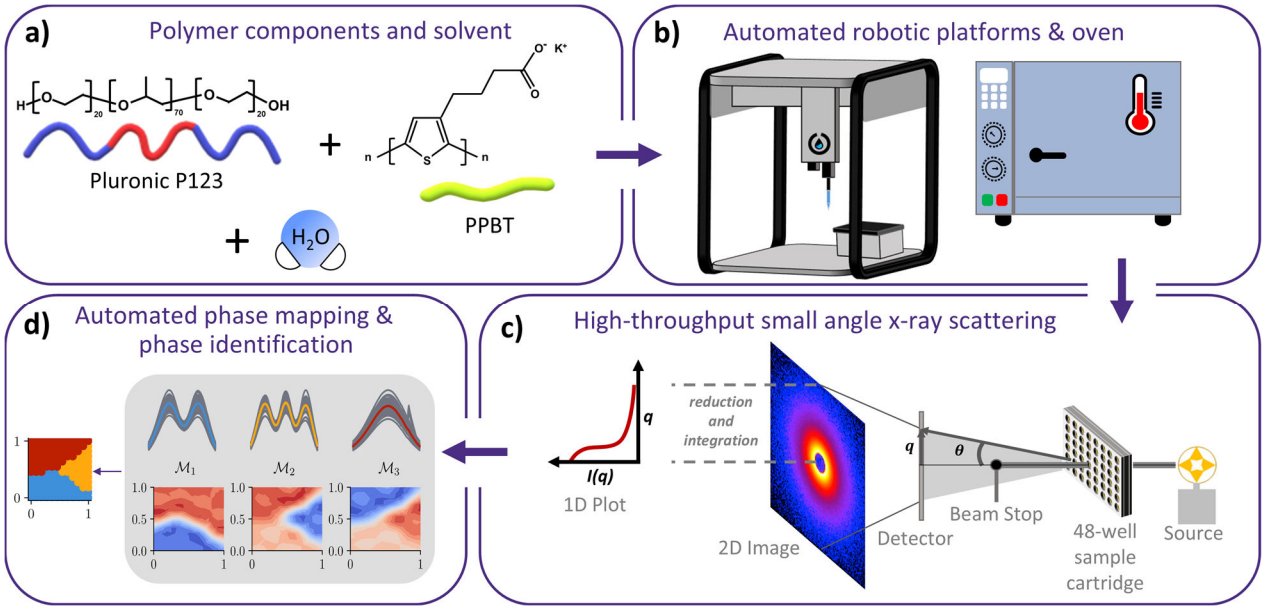

Figure 1. Structural characterization of block copolymer and conjugated polymer blends. (a) Structure of blend components including Pluronic P123, PPBT, and water. (b) The polymer components and solvent are mixed and dried using an automated liquid handling robot and oven. The necessary amount of water is then added to achieve the final desired concentration after complete mixing. (c) Samples are loaded in a 48-well plate cartridge with Kapton windows and SAXS is performed at room temperature. Scattered x-rays are collected at the detector and a 2D image is created that is then reduced and integrated to obtain a 1D profile. (d) A phase map is then automatically learned and generated from the 1D SAXS spectra and each phase identified through analysis of the profiles and the Bragg peak ratios.

Rheological Small Angle Neutron Scattering (SANS)

In-situ Rheo-SANS was used to investigate the effect of shear alignment of Pluronic P123-PPBT blends forming ordered mesophases. Shear orientation experiments were performed using the Quokka 40 m long SANS instrument at the Australian Nuclear Science and Technology Organization (ANSTO)[40] . A neat 30 wt% Pluronic P123 in D_2O, and a blend of 30 wt% Pluronic P123 and 1 wt% PPBT in D_2O were loaded in separate experiments into a bob and cup Couette cell with a stationary 50mm quartz cup and 49mm titanium bob (**Fig. S1**) on an Anton Paar MCR 302e stress control rheometer (North Ryde, NSW). The 1.0mm thick samples were sheared at rates 0 s^{-1}, 10 s^{-1}, and 100 $s^{-}1$ at 35°C before increasing the temperature to 45°C. Two-dimensional (2D) profiles were obtained at a sample-to-detector distance (SDD) of 4 m in the radial direction. The NCNR SANS reduction macro[41] for Igor Pro was used to reduce the data, integrating 2D scattering images to 1D profiles, correcting for the instrument background, subtract empty shear cell background, and to determine absolute scaling of scattering intensity. For 2D images with Bragg spots, the azimuthal average of the first ring was obtained using SasView 5.0.4.

Results and Discussion

Effect of Concentration on Polymer blend morphology

To characterize the effects of PPBT on the phase behavior of the Pluronic P123 hydrogel system, SAXS measurements of neat Pluronic P123 and of blends of Pluronic P123 with increasing concentrations of PPBT were performed at 23°C. As mentioned previously, Pluronic aqueous solutions are known to form isotropic micelles at low concentrations (5-25 wt%) as denoted by broad oscillating profiles in the SAXS curves (**Fig. 2a**). These samples are fluid and do not sustain their weight when their container is inverted. SAXS profiles of dilute Pluronic P123 samples show a horizonal slope (Guinier region) at low-q, which is suggestive of micelle formation. The addition of the CP component (PPBT) to the Pluronic P123 at low concentrations is found to significantly affect the micellar shape as indicated by the changes in the scattering at low-q. Blends at dilute conditions, 5-25 wt% Pluronic P123 and 1 wt% PPBT, are also fluid and show signatures of isotropic micelles (**Fig. 2b**). However, scattering at low-q has a larger negative slope (i.e. no Guinier region is evident), demonstrating that the micelle shape is modified to form elongated structures.

At high concentrations, neat Pluronic P123 and co-assemblies of Pluronic P123 with PPBT exhibit several clearly defined peaks. These Bragg peaks are characteristic of crystalline mesophases commonly observed in Pluronic P123. Crystal structures can be identified by quantification of the ratios of Bragg peaks observed in the SAXS data. However, it must be noted that multiple phases may coexist in a given sample and peak intensities may also be affected by the form-factor of the micellar subunits that makeup the structures. Single-phase structures identified in self-assembled samples are face-centered cubic crystals (FCC) of spherical micelles $[1, \sqrt{4/3}, \sqrt{8/3}, \sqrt{11/3}, \sqrt{12/3}, \sqrt{16/3}, \dots]$, hexagonally closed packed cubic crystals (HCP) [1,

1.06, 1.13, 1.46, 1.73, …] of spherical micelles, and hexagonal crystals (HEX) $[1, \sqrt{3}, \sqrt{4}, \sqrt{7}, \sqrt{9}, \sqrt{12}, \ldots]$ of cylindrical micelles [42,43]. Neat P123 transitions from FCC (25-30 wt%) to HCP (35 wt%), and finally a mix of HCP and HEX (40 wt%). With the addition of 1 wt% PPBT, the structure transition was altered to isotropic micelles (25wt%), FCC (30wt%), and finally HEX (35-40 wt%). It is clear from the mesophase transitions that the addition of PPBT shifts mesophase assembly toward elongated structures.

Observation of crystallization in blends of Pluronic P123 with PPBT demonstrates that the CP additive does not prevent self-assembly, but it may still modify the structure of the composite mesophases that are formed. **Fig. 2c** shows SAXS intensities of Pluronic P123 with increasing concentrations of PPBT to clearly demonstrate the effect of CP concentration on phase transitions between mesophases. At this concentration (35 wt%) Pluronic P123 self-assembles into an FCC and HCP mixed phase that persists until ~1 wt% of PPBT is added. Even at very low concentrations of PPBT (~0.1 wt%), the effect of the CP additive at low-q becomes obvious with an increasing negative slope in the log-log plot that is indicative of structural changes emerging at larger length scales. At even higher concentrations of PPBT (~ 1wt%), the structure of the polymer blend begins to shift from cubic (FCC/HCP) to HEX as noted by the Bragg peak spacings. However, at even higher concentrations of PPBT (> 4wt% PPBT) the hexagonal cylinders (HEX) become increasingly disorganized and secondary peaks are eventually lost. At loadings of PPBT of 5 wt% and above, the primary correlation peak is still evident, suggesting strong correlations, but subsequent peaks disappear and a broad correlation feature at high-q (~0.15 $Å^{-1}$) that is characteristic of polyelectrolytes becomes prominent[44,45]. Crystalline organization at mesoscale length scales is lost at high PPBT loadings.

As the PPBT loading increases, peaks in SAXS profiles also shift to lower q, which corresponds to an increase in the lattice parameter. The micelle diameter of each phase was inferred and calculated from the 1^{rst}-order Bragg peak q_1 using the following relationships: $\frac{\pi\sqrt{6}}{q_1}$ for FCC, $\frac{4\pi}{q_1\sqrt{3}}$ for HCP and $\frac{4\pi}{q_1\sqrt{3}}$ for HEX, respectively[25]. The micelle diameter of neat P123 at 35 wt% (inferred from the lattice spacing) is 18.2 nm for cubic (FCC and HCP) domains. This diameter increases with PPBT concentration until reaching 18.6 nm for FCC domains at 0.5 wt% PPBT. The cylindrical micelles of the blend at 1 wt% PPBT (HEX) have a diameter of 17.0 nm. The decrease in micelle size is likely due to the new packing structure of a hexagonal cylinder. The micelles diameter then continues increasing with PPBT concentration until reaching 18.1 nm concentration at 5 wt% PPBT. The swelling of micelles is indicative of PPBT being incorporated into the micelle cores. Although the side-chains are charged and hydrophilic, PPBT still has a hydrophobic backbone that is expected to be more compatible with the hydrophobic PPO micelle cores of P123. Moreover, the structural transition from cubic (FCC/HCP) to cylindrical micelles (HEX) upon addition of increasing amounts of PPBT is suggestive of integration of the CP into the hydrophobic Pluronic micelle core.

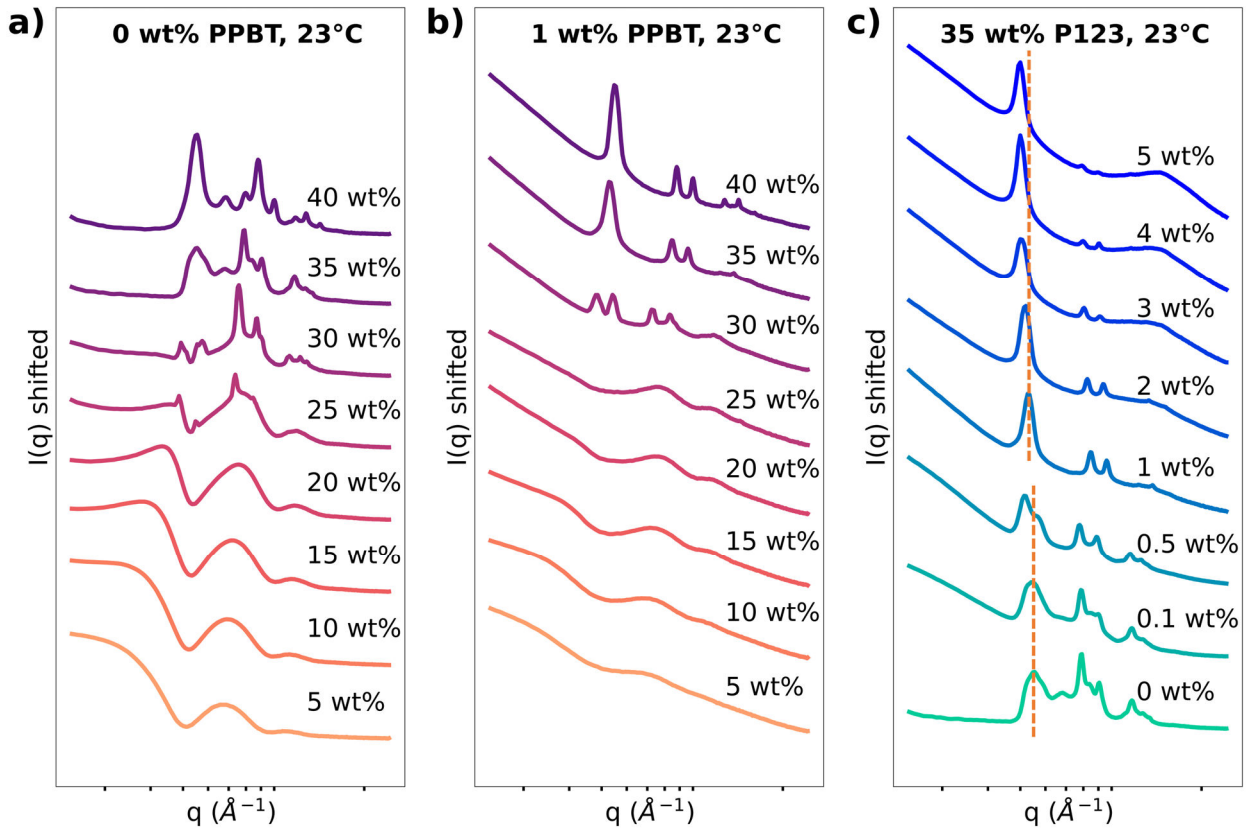

Figure 2. 1D SAXS profiles of (a) increasing concentrations of P123, (b) blends with 1 wt% PPBT with increasing P123 concentration, and (c)blends with 35 wt% P123 with increasing PPBT. From 0 to 0.5 wt% PPBT the dashed lines show the 3rd peak of hexagonal close packed sphere (HCP) structure shift to lower q as PPBT concentration increases. From 1 to 5 wt% PPBT the dashed lines show the 1st peak of hexagonally packed cylinders (HEX) structure shift to lower q as PPBT concentration increases. The scattering intensities are shifted vertically for visual clarity.

A phase map was automatically generated using the HT-SAXS data and the *autophasemap* algorithm with four template functions (in solid color) and an interpolated probability threshold of 0.3 (**Fig. 3**). The design space is separated into phase regions highlighted in the inset plot in each panel with the concentration of Pluronic P123 on the x-axis (ranging from 0-40 wt%) and concentration of PPBT on the y-axis (ranging from 0-5 wt%). Blends classified under the template

with broad oscillating peaks were classified as a micellar solution with little long-range order (**Fig. 3a**). The remaining template functions exhibit Bragg peaks that are indicative of micelles assembling into a semicrystalline structure of different kinds. These template functions roughly correspond to an FCC-like structure (**Fig. 3b**), a mixed-phase HEX structure with HCP influence with peak spacing ratios (**Fig. 3c**), and primarily HEX structures with peak spacing ratios (**Fig. 3d**). Overlapping regions of the phase map are the result of the probability exceeding the minimum threshold for more than one template. On the other hand, empty regions appear when probability factors do not meet the threshold of any phase (**Fig. 3e**). The *autophasemap* process is based on unsupervised statistical analysis, thus it is expected for the template families to contain a few outlier profiles. These outlier profiles also alter the shape of the template itself, thus representative SAXS curves are provided for each phase in **Fig. S2**. Although *autophasemap* may misclassify some SAXS curves, the general trends observed from *autophasemap* are valid and based on ensembles of data with significant sampling. A phase map of manually analyzed SAXS data is provided in **Fig. S7** for comparison. It is evident from SAXS and autogenerated phase maps that the presence of PPBT induces a shift in Pluronic P123 crystal structure from the cubic phases to hexagonal cylinders due to the rigidity of the conjugated polymer.

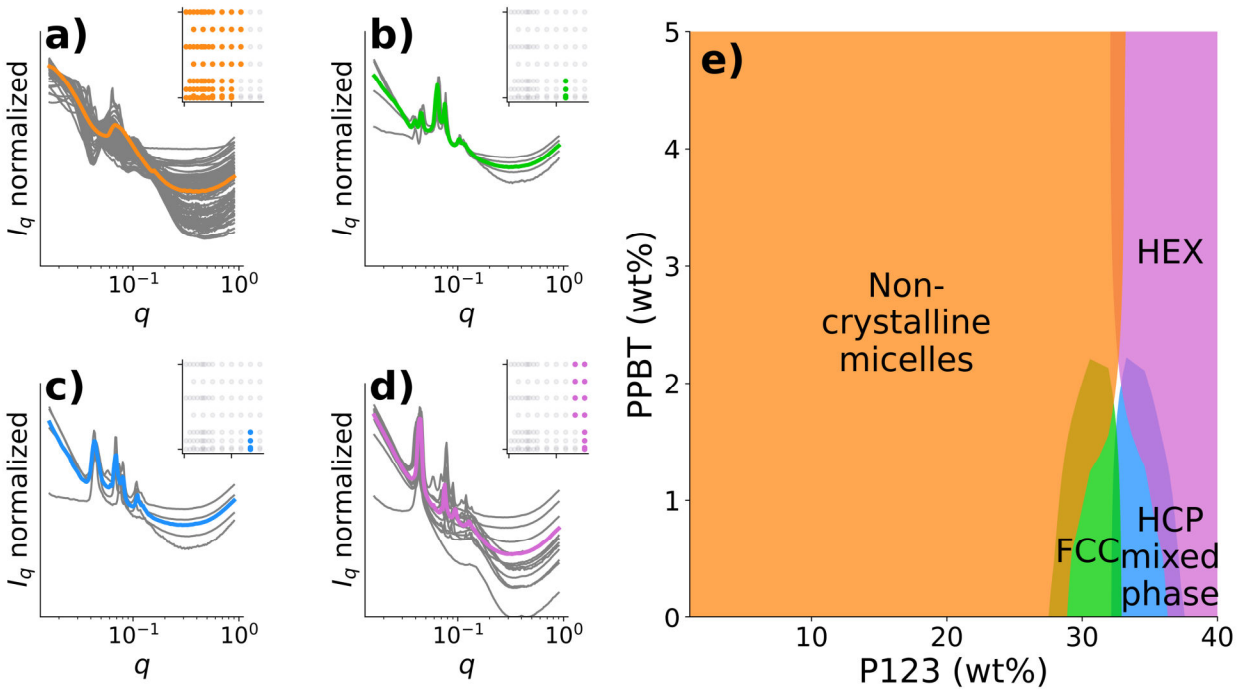

Figure 3. A phase map learned with 4 templates for blend samples with varying concentrations of P123 and PPBT at room temperature. (a-d) 1D SAXS profiles (grey) assigned to each learned template (color). The inserts depict the corresponding region of SAXS profiles in the composition space, with the x-axis representing P123 wt% and y-axis representing PPBT wt%. (e) A phase map obtained by determining regions of similarity between SAXS profile and template. Each phase region corresponds to the template of the same color.

Effect of Temperature on Polymer blend morphology

The effects of temperature on the phase behavior of the Pluronic P123 and PPBT blends was also characterized through SAXS. The blends show a similar phase transition to neat Pluronic P123 samples but with an increased hexagonal cylindrical (HEX) phase at lower temperatures due to the presence of PPBT. This observation is highlighted in the 1D SAXS profiles of neat Pluronic P123 at 35 wt% in comparison to blends of 35 wt% Pluronic P123 and 1 wt% PPBT (**Fig. 4**). At 0 °C, neat Pluronic P123 micelles are more organized than isotropic micelles but not as organized

as a lyotropic liquid crystal. P123 then exhibits an HCP structure between 10-30℃. At 40-50℃, the SAXS data exhibits mostly hexagonal cylinder Bragg peaks, but some HCP features remain at 40℃. At 60℃ and above, the semicrystalline structure of P123 has become disorganized (**Fig. 4a**). Blends at 0℃ show correlated micelles that have not yet organized into a lyotropic liquid crystal but show strong interaction. The blends then exhibit an HCP structure between 10-20℃. At 30-60℃, the SAXS data exhibits hexagonal cylinder Bragg peaks, 10 degrees lower than their neat P123 counterpart. Similarly to their neat P123 counterparts, the semicrystalline structure of P123 has become disorganized at 60℃ and above (**Fig. 4b**).

Peaks of 1D SAXS profiles for neat P123 shift to lower q with increasing temperature, which corresponds to an increase in micelle size (**Fig 4a**). P123 blends with PPBT also shifts to lower q with increasing temperature (**Fig 4b**). The micelle diameter of neat 35 wt% P123 is 17.2 nm for both FCC and HCP at 10℃ and gradually increases with temperature until reaching 20.4 nm for HEX at 50℃. The micelles of the blends at 10℃ have a diameter of 17.3 nm for both FCC and HCP and increases to 20.4 nm for HEX at 50℃. This increase in micelle size alludes to conformational changes of the polymers due to temperature-related desolvatation[28,29]. In addition, the swelling of micelles with increasing PPBT concentration agrees with previously observed behavior of blends.

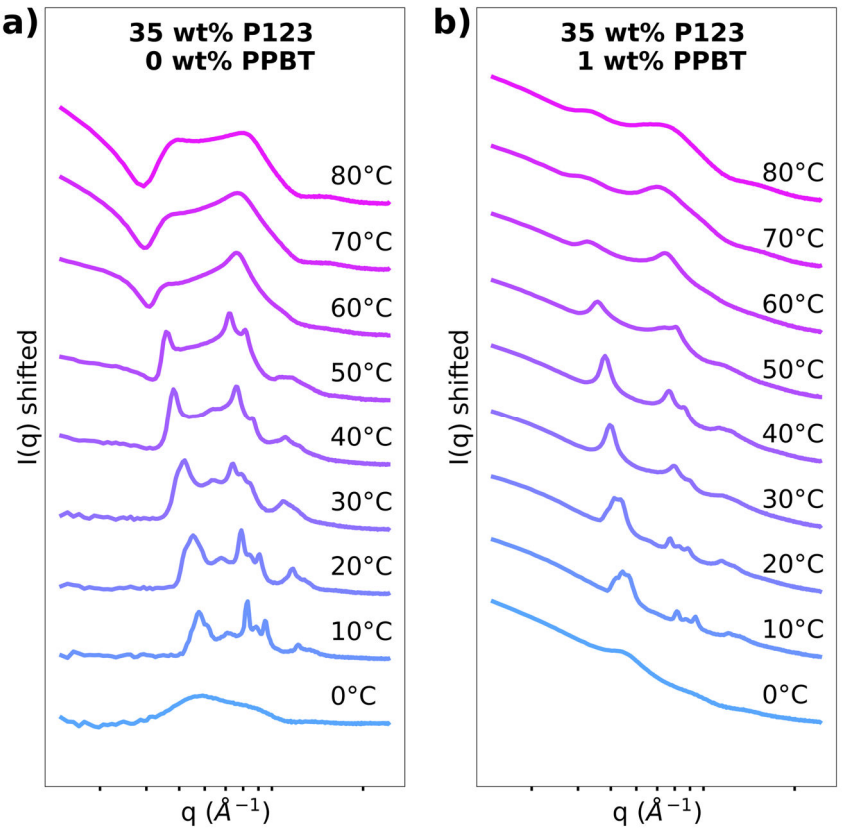

Figure 4. 1D SAXS profiles of (a) 35 wt% neat P123 and (b) a blend of 35 wt% P123 and 1wt% PPBT at varying temperature. The scattering intensities are shifted vertically for visual clarity.

A phase map was also automatically generated using *autophasemap* with five template functions and an interpolated probability threshold of 0.3 for neat P123 as a function of temperature. The design space is partitioned into phase regions with the concentration of P123 on the x-axis (ranging from 0-40 wt%) and temperature on the y-axis (ranging from 0-85°C) (**Fig. 5**). The template functions of neat P123 roughly correspond to micelles in solution (**Fig. 5a**), disordered (**Fig. 5b**), FCC (**Fig. 5c**), a mixed phase of HCP and HEX (Fig. 5d), and HEX with a degree of disorder (**Fig. 5e**). 'Disordered' refers to a phase in which micelles have no long-range order as evidenced by a lack of sharp peaks in their SAXS curve. Representative SAXS curves are shown for each phase in **Fig. S3**. The phase transition depicted on the phase map closely

corresponds to the SAXS intensities observed for 35wt% P123 (**Fig. 4a**), with the sample progressing from correlated micelles, a cubic structure containing FCC, a hexagonal structure, and finally to disordered. A phase map of manually analyzed SAXS data is provided in **Fig S8a** for comparison.

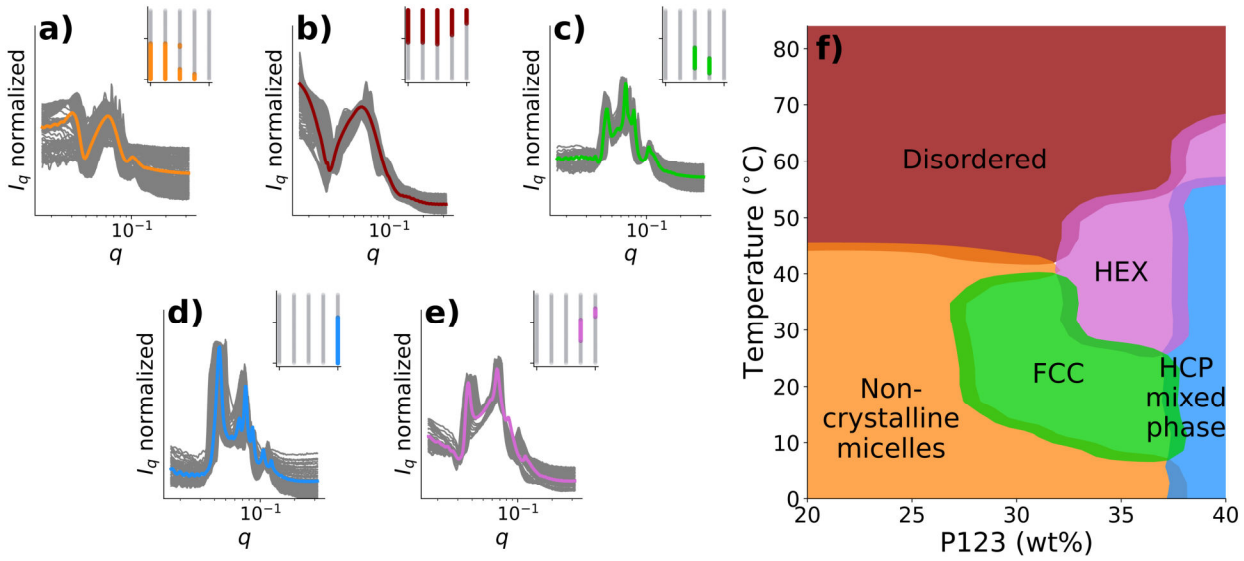

Figure 5. A phase map learned with 5 templates for samples of 20-40 wt% neat P123 from 0-100°C. (a-e) 1D SAXS profiles (grey) assigned to each learned template (color). The inserts depict the corresponding region of SAXS profiles in the composition space, with the x-axis representing P123 wt% and y-axis representing temperature. (f) A phase map obtained by determining regions of similarity between SAXS profile and template. Each phase region corresponds to the template of the same color.

A phase map was generated for a 35 wt% P123 and 1 wt% PPBT blend similar to the previous one with seven template functions and a threshold of 0.3. The design space was also partitioned into phase regions with the concentration of P123 on the x-axis (ranging from 0-40 wt%) and temperature on the y-axis (ranging from 0-85°C) (**Fig. 6**). A notable difference of these template functions in comparison to the ones for neat P123 is the negative slope at low q due to

the long PPBT. Template functions of this blend roughly correspond to amorphous micelle solutions (**Fig. 6a**), FCC (**Fig. 6b**), a mixed phase of HCP and HEX (**Fig. 6c**), HEX (**Fig. 6d**), and a disorganized phase (**Fig. 6e**). The disorganized phase contains sharp peaks but does not follow the peak spacing of any crystalline structure. The micellar region encompasses a substantial section of the phase map and exhibits broad oscillating peaks. However, the features defined by these broad oscillating peaks are ambiguous. Isotropic micelles, polyelectrolytes, and correlated micelles are all characterized by broad peaks in SAXS curves (**Fig. S5**), which makes it difficult for *autophasemap* to differentiate these phases. The transition between crystalline phases at 35 wt% P123 also broadly agrees with the SAXS intensities of the blend (**Fig. 4b**). The sample shows an HCP structure between 10-20°C, as reflected in the template function (**Fig. 6d**), but the template function also includes HEX features. The crystalline structure of the blend subsequently moves to HEX and eventually a disorganized phase, also indicated by the corresponding template functions. Phase representative SAXS data is shown in **Fig S4** and a phase map of manually analyzed SAXS data is provided in **Fig S8b** for comparison. A region of uncertainty exists between the FCC-like and disorganized phases. At first glance, the FCC and disorganized templates look similar with two clear high intensity features. However, upon closer inspection, the FCC phase shows two peaks in each feature (**Fig S6a**), whereas the disorganized phase only has one peak each (**Fig S6b**). We believe this is a limitation of *autophasemap* stemming from the limited sampling of the FCC phase that spans along the direction where the data sampling is sparse.

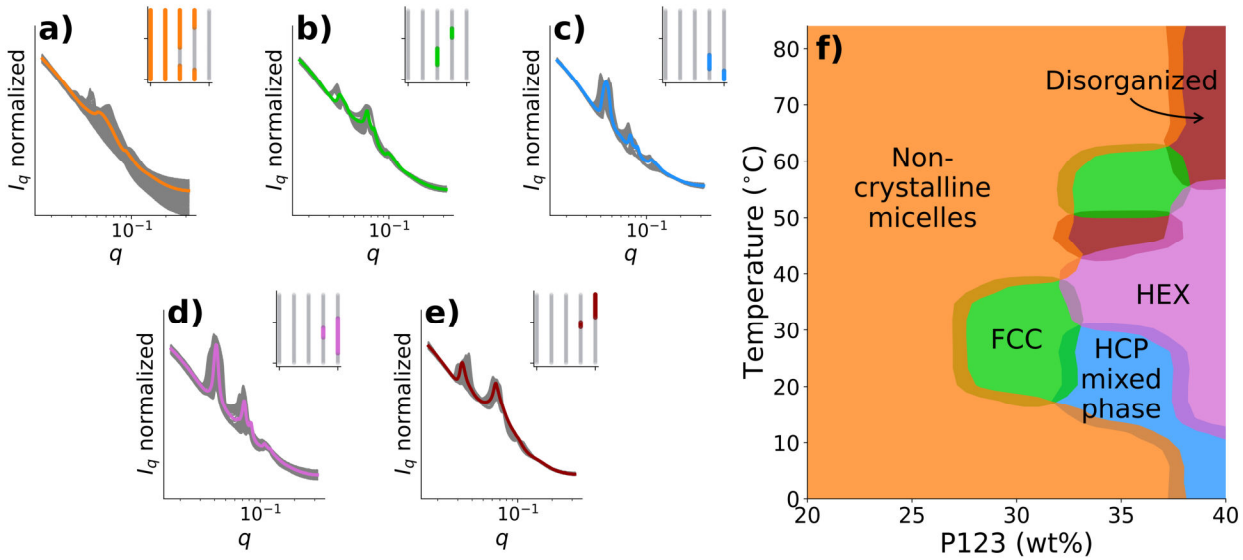

Figure 6. A phase map learned with 5 templates for blends of 20-40 wt% P123 and 1 wt% PPBT from 0-100°C. (a-e) 1D SAXS profiles (grey) assigned to each learned template (color). The inserts depict the corresponding region of SAXS profiles in the composition space, with the x-axis representing P123 wt% and y-axis representing temperature. The black arrows point to high-intensity features of that phase. (f) A phase map obtained by determining regions of similarity between SAXS profile and template. Each phase region corresponds to the template of the same color.

Effect of Shear on Polymer blend morphology

Shear alignment can refine the organization of a material into a single crystalline phase, presenting an opportunity to optimize its overall performance and functionality. Therefore, it is of interest to demonstrate this alignment in our BCP and CP blend system. Shearing PEO-PPO-PEO hydrogels is known to induce the annealing of defects and the organization of micelles into single-crystalline domains. To determine the impact of PPBT on the shear-induced phase behavior of the polymer system, neat 30wt% P123 and a blend of 30wt% P123 and 1wt% PPBT at various shear conditions were analyzed. These measurements were first conducted at 35 °C at 0 s^{-1}, 10 s^{-1}, and

100 s^{-1}. The temperature of each sample is then increased to 45 ℃ and measured at 0 s^{-1}, 10 s^{-1}, and 100 s^{-1}. The shear history is retained throughout each condition but does not impede the conclusion that monolithic crystal structures form through shear.

The 2D SANS profile of P123 at 35 ℃ shows isotropic concentric rings which are the signature of powder-like behavior (**Fig. 7a**). When shear at 10s^{-1} is applied to the hydrogel, Bragg spots begin to appear in hexagonal rings (**Fig. 7b**). In the innermost ring the spots at φ = 90° and 270° are more intense than the other four spots as seen in the azimuthal average. This anisotropy is most likely due to the stable coexistence of more than one crystal orientation. At a high shear rate of 100s^{-1} multiple hexagonal rings have become clear and symmetrical (**Fig. 7c**), indicating the micelles have organized into a single-crystalline domain. The hexagonal rings are the signature of a cubic structure, most likely a mixture of HCP and FCC. The neat P123 sample at 45℃ shows less monolithic structures. The sample without shear still exhibits hexagonal rings but much less intense (**Fig. 7d**), which indicates the structure was retained from the single-crystalline cubic crystal formed at 35 ℃. Applying 10 s^{-1} removes any Bragg spots, but this may be due to a transition between phases (Fig. 8e). At 100 s^{-1}, the 2D profile and azimuthal average shows faint Bragg spots at φ = 90° and 270° (**Fig. 7f**), portraying a shift to an elongated structure. Based on the position of the peaks of the sector average at φ = 90° (**Fig S9**), the elongated structure is HEX.

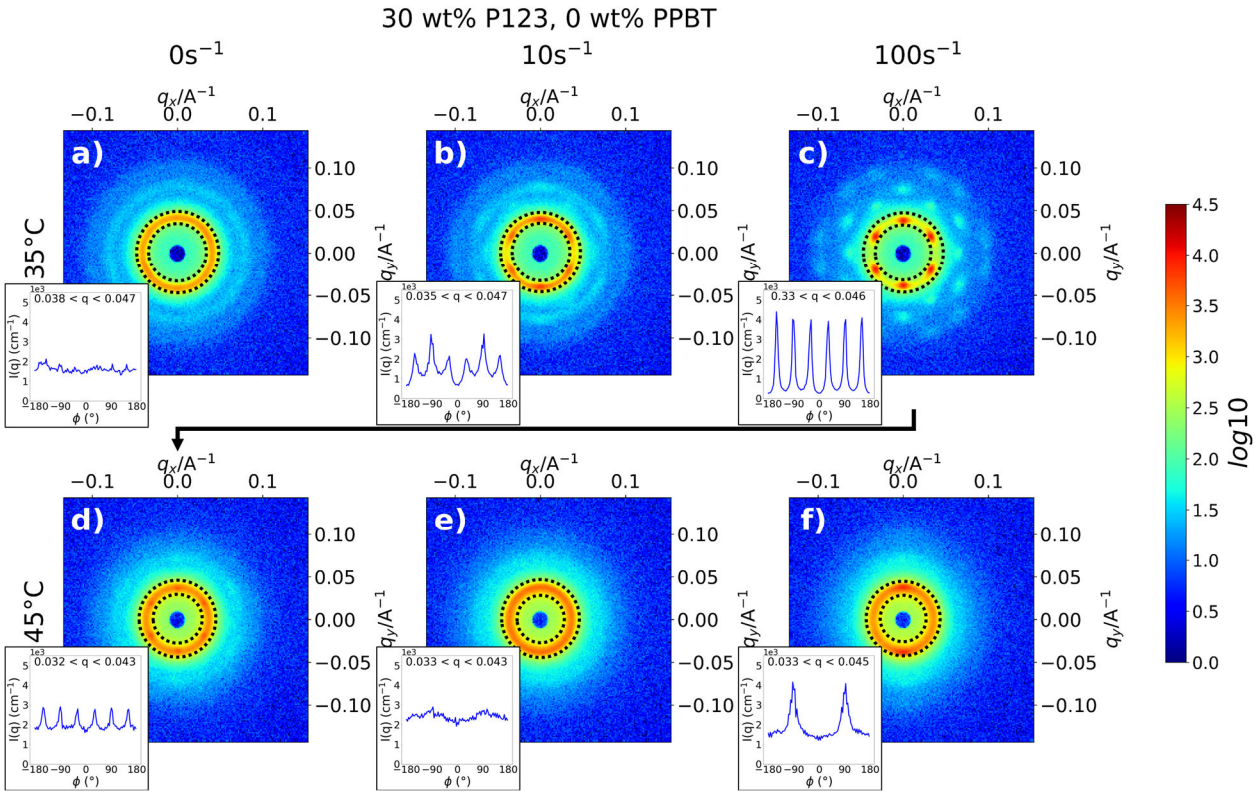

Figure 7. Neat P123 at 35°C and sheared at (a) 0 s^{-1}, (b) 10 s^{-1}, and (c) 100 s^{-1}. P123 is subsequently heated to 45°C and sheared at (d) 0 s^{-1}, (e) 10 s^{-1}, and (f) 100 s^{-1}. Inserts depict the azimuthal average between the indicated q-ranges of the innermost Bragg spots. The q-range is represented by black dotted rings.

The phase transition from cubic to hexagonal structure for the blend of 30 wt% P123 and 1 wt% PPBT is notably different from its neat P123 counterpart. At 35 °C, the blend also does not show a single crystalline structure at rest (**Fig. 8a**). However, unlike the neat P123 sample, the blend at 10 s^{-1} exhibits a clear single crystalline cubic structure as determined by the multiple hexagonal rings in the 2D profile, and the azimuthal average of the first ring show intense and uniform peaks (**Fig. 8b**). Furthermore, at 100 s^{-1} the hexagonal rings have become disordered and asymmetrical with the azimuthal average showing slightly more intense Bragg spots at φ = 90°

and 270°, indicating high shear induced anisotropy in the structure (**Fig. 8c**). When the blend was heated to 45 °C the 2D SANS profile only depicts isotropic concentric rings (**Fig. 8d**). At $10s^{-1}$, the structure is starting to shift to hexagonal cylinders as indicated by the faint Bragg spots at φ = 90° and 270° and short broad peaks in the azimuthal average (**Fig. 8e**). This type of structure did not occur for neat P123 until sheared at 100 s^{-1}. A single crystalline HEX phase has formed at 100 s^{-1}, highlighted by clear Bragg spots and sharp and intense azimuthal average peaks (**Fig. 8f**). Compared to the sample at the initial 35 °C, the structure of the blend became more prominent at high shear. This would indicate that the rigidity of PPBT at high shear rates is detrimental for single crystalline cubic structures while enhancing elongated ones.

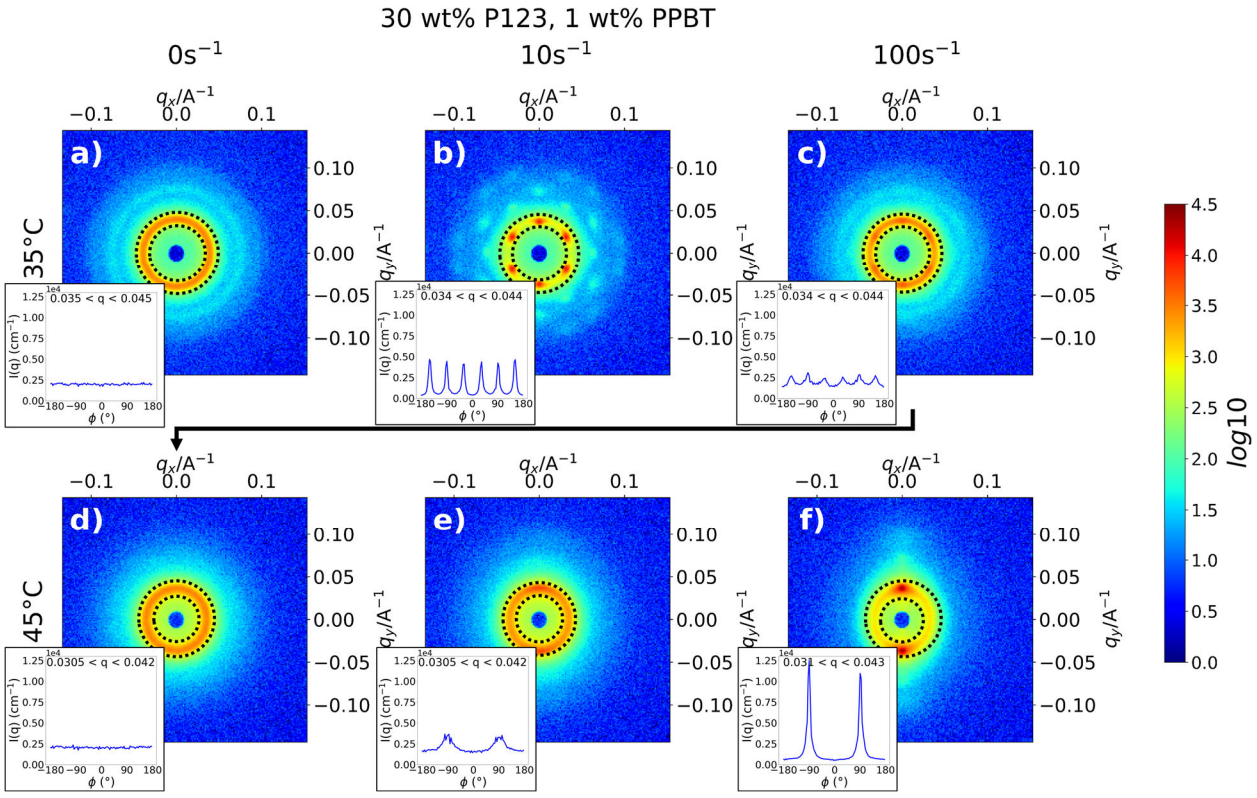

Figure 8. Blend of 30 wt% P123 and 1 wt% PPBT at 35 °C and sheared at (a) 0 s^{-1}, (b) 10 s^{-1}, and (c) 100 s^{-1}. P123 is subsequently heated to 45 °C and sheared at (d) 0 s^{-1}, (e) 10 s^{-1}, and (f) 100 s^{-}

[1]. Inserts depict the azimuthal average between the indicated q-ranges of the innermost Bragg spots. The q-range is represented by black dotted rings.

Conclusion

In this work we report the effects of PPBT on the phase behavior of self-assembling Pluronic P123. P123 from 5 to 40 wt% in aqueous solutions show a lyotropic phase transition from isotropic micelles, FCC, HCP, and finally a mixed phase of HCP and HEX. The crystalline structure of the polymer blend shifts fully to HEX as the concentration of PPBT increased. At high concentrations, PPBT disrupts the organization of P123 micelles. Aqueous solutions of 35 wt% P123 from 5 to 80 °C change from correlated micelles, HCP, HEX, to a disordered phase. Blends with P123 and PPBT exhibit similar crystalline structures but the shift to a hexagonal cylinder phase is observed at lower temperatures in the presence of PPBT and maintained over broader temperature ranges. The favoring of elongated nanostructures also occurs shear-induced monolithic crystal structures. When highly sheared at 35 °C, neat P123 assembles into a single crystalline cubic structure. At high shear and 45 °C, P123 only shows a still developing single crystalline HEX phase. The blend of P123 and PPBT showed a single crystalline cubic structure at low shear and 35 °C, and a fully single crystalline HEX structure at high shear and 45 °C. Co-assemblies of BCP and CP may provide a scalable and simple fabrication process for novel materials with long range order without the need of complex polymerizations. If properly orientated, these anisotropic materials have the potential to enhance applications in optical sensors, bioelectronic interfaces, flexible electronics, and more. Additional research is needed to establish the connection between the morphologies and properties of these highly order co-assemblies. However, this study serves as the groundwork for understanding the use of blends to tune the structure of semi-crystal forming BCPs and conductive CP.

Supporting Information

Supporting Information: Additional figures and details of representative SAXS curves, limitations of *autophasemap* and comparison to manual analysis, and sheared elongated structure (PDF)

Acknowledgements

Primary support for this work was provided by the Department of Energy Office of Basic Energy Sciences under award no. DE-SC0019911, which directly supported the research participation of all authors and the procurement of materials. This research used resources of the Advanced Photon Source, a U.S. Department of Energy (DOE) Office of Science User Facility operated for the DOE Office of Science by Argonne National Laboratory under contract no. DE-AC02-06CH11357. We would like to thank the Australian Nuclear Science and Technology Organisation (ANSTO) for providing the neutron research facilities used in this work at the Open-pool Australian lightwater reactor (OPAL) under proposal no. 15774. This work relied on the SasView application, originally developed under NSF award DMR-0520547. SasView contains code developed with funding from the European Union's Horizon 2020 research and innovation program under the SINE2020 project, grant agreement no. 654000.

References

1. A. Mazzio, K. & K. Luscombe, C. The future of organic photovoltaics. *Chem. Soc. Rev.* **44**, 78–90 (2015).

2. Paulsen, B. D., Tybrandt, K., Stavrinidou, E. & Rivnay, J. Organic mixed ionic–electronic conductors. *Nat. Mater.* **19**, 13–26 (2020).

3. Simon, D. T., Gabrielsson, E. O., Tybrandt, K. & Berggren, M. Organic Bioelectronics: Bridging the Signaling Gap between Biology and Technology. *Chem. Rev.* **116**, 13009–13041 (2016).

4. Liu, K., Ouyang, B., Guo, X., Guo, Y. & Liu, Y. Advances in flexible organic field-effect transistors and their applications for flexible electronics. *Npj Flex. Electron.* **6**, 1–19 (2022).

5. Chen, H.-W., Lee, J.-H., Lin, B.-Y., Chen, S. & Wu, S.-T. Liquid crystal display and organic light-emitting diode display: present status and future perspectives. *Light Sci. Appl.* **7**, 17168–17168 (2018).

6. Chow, P. C. Y. & Someya, T. Organic Photodetectors for Next-Generation Wearable Electronics. *Adv. Mater.* **32**, 1902045 (2020).

7. Cao, Z., Leng, M., Cao, Y., Gu, X. & Fang, L. How rigid are conjugated non-ladder and ladder polymers? *J. Polym. Sci.* **60**, 298–310 (2022).

8. Nikolka, M. *et al.* High-mobility, trap-free charge transport in conjugated polymer diodes. *Nat. Commun.* **10**, 2122 (2019).

9. Li, X. & Chen, G. Effect of interchain coupling on the excited polaron in conjugated polymers. *Phys. Lett. A* **381**, 549–555 (2017).

10. Goffri, S. *et al.* Multicomponent semiconducting polymer systems with low crystallization-induced percolation threshold. *Nat. Mater.* **5**, 950–956 (2006).

11. Qiu, L. *et al.* Organic Thin-film Transistors Based on Polythiophene Nanowires Embedded in Insulating Polymer. *Adv. Mater.* **21**, 1349–1353 (2009).

12. Sarkar, B. & Alexandridis, P. Block copolymer–nanoparticle composites: Structure, functional properties, and processing. *Prog. Polym. Sci.* **40**, 33–62 (2015).

13. Wolf, C. M. *et al.* Blend Morphology in Polythiophene–Polystyrene Composites from Neutron and X-ray Scattering. *Macromolecules* **54**, 2960–2978 (2021).

14. Soni, S. S., Fadadu, K. B. & Gibaud, A. Ionic Conductivity through Thermoresponsive Polymer Gel: Ordering Matters. *Langmuir* **28**, 751–756 (2012).

15. Alexandridis, P. & Alan Hatton, T. Poly(ethylene oxide)-poly(propylene oxide)-poly(ethylene oxide) block copolymer surfactants in aqueous solutions and at interfaces: thermodynamics, structure, dynamics, and modeling. *Colloids Surf. Physicochem. Eng. Asp.* **96**, 1–46 (1995).

16. Alexandridis, P., Holzwarth, J. F. & Hatton, T. A. Micellization of Poly(ethylene oxide)-Poly(propylene oxide)-Poly(ethylene oxide) Triblock Copolymers in Aqueous Solutions: Thermodynamics of Copolymer Association. *Macromolecules* **27**, 2414–2425 (1994).

17. Wanka, G., Hoffmann, H. & Ulbricht, W. Phase Diagrams and Aggregation Behavior of Poly(oxyethylene)-Poly(oxypropylene)-Poly(oxyethylene) Triblock Copolymers in Aqueous Solutions. *Macromolecules* **27**, 4145–4159 (1994).

18. Jang, H.-S., Kim, T.-H., Do, C., Lee, M.-J. & Choi, S.-M. Single-walled carbon nanotube induced re-entrant hexagonal phases in a Pluronic block copolymer system. *Soft Matter* **9**, 3050–3056 (2013).

19. Pozzo, D. C. & Walker, L. M. Macroscopic alignment of nanoparticle arrays in soft crystals of cubic and cylindrical polymer micelles. *Eur. Phys. J. E* **26**, 183–189 (2008).

20. Xie, L. & Zhu, Y. Tune the phase morphology to design conductive polymer composites: A review. *Polym. Compos.* **39**, 2985–2996 (2018).

21. Onorato, J. W. & Luscombe, C. K. Morphological effects on polymeric mixed ionic/electronic conductors. *Mol. Syst. Des. Eng.* **4**, 310–324 (2019).

22. Na, R. *et al.* A Robust Conductive Polymer Network as a Multi-Functional Binder and Conductive Additive for Supercapacitors. *ChemElectroChem* **7**, 3056–3064 (2020).

23. Lenaerts, V., Triqueneaux, C., Quartern, M., Rieg-Falson, F. & Couvreur, P. Temperature-dependent rheological behavior of Pluronic F-127 aqueous solutions. *Int. J. Pharm.* **39**, 121–127 (1987).

24. Pozzo, D. C., Hollabaugh, K. R. & Walker, L. M. Rheology and phase behavior of copolymer-templated nanocomposite materials. *J. Rheol.* **49**, 759–782 (2005).

25. Soni, S. S., Brotons, G., Bellour, M., Narayanan, T. & Gibaud, A. Quantitative SAXS Analysis of the P123/Water/Ethanol Ternary Phase Diagram. *J. Phys. Chem. B* **110**, 15157–15165 (2006).

26. Albouy, P. A. *et al.* Freezing-induced self-assembly of amphiphilic molecules. *Soft Matter* **13**, 1759–1763 (2017).

27. Han, L., Guo, J., Zhang, L., Wang, Q. & Fang, X. Pharmacokinetics and biodistribution of polymeric micelles of paclitaxel with Pluronic P123. *Acta Pharmacol. Sin.* **27**, 747–753 (2006).

28. Wolff, N., Gerth, S., Gutfreund, P. & Wolff, M. Temperature dependent cubic and hexagonal close packing in micellar structures. *Soft Matter* **10**, 8420–8426 (2014).

29. Shriky, B. *et al.* Pluronic F127 thermosensitive injectable smart hydrogels for controlled drug delivery system development. *J. Colloid Interface Sci.* **565**, 119–130 (2020).

30. Grocke, G. L. *et al.* Structure–Transport Properties Governing the Interplay in Humidity-Dependent Mixed Ionic and Electronic Conduction of Conjugated Polyelectrolytes. *ACS Polym. Au* **2**, 275–286 (2022).

31. Risteen, B. E. *et al.* Enhanced Alignment of Water-Soluble Polythiophene Using Cellulose Nanocrystals as a Liquid Crystal Template. *Biomacromolecules* **18**, 1556–1562 (2017).

32. Das, P. *et al.* Evaluating the Impact of Conjugation Break Spacer Incorporation in Poly(3,4-propylenedioxythiophene)-Based Cathode Binders for Lithium-Ion Batteries. *Chem. Mater.* **36**, 1413–1427 (2024).

33. Wang, M., Baek, P., Akbarinejad, A., Barker, D. & Travas-Sejdic, J. Conjugated polymers and composites for stretchable organic electronics. *J. Mater. Chem. C* **7**, 5534–5552 (2019).

34. Marks, A., Griggs, S., Gasparini, N. & Moser, M. Organic Electrochemical Transistors: An Emerging Technology for Biosensing. *Adv. Mater. Interfaces* **9**, 2102039 (2022).

35. Pozzo, L. Automation-Hardware/Cartridge Sample Holder for SAS Experiments/SAXS-USAXS Liquids 48 well plate holder at master · pozzo-research-group/Automation-Hardware. *GitHub* https://github.com/pozzo-research-group/Automation-Hardware.

36. Vaddi, K., Li, K. & Pozzo, L. D. Metric geometry tools for automatic structure phase map generation. *Digit. Discov.* **2**, 1471–1483 (2023).

37. papers/autophasemap at main · pozzo-research-group/papers. *GitHub* https://github.com/pozzo-research-group/papers/tree/main/autophasemap.

38. Arthur, D. & Vassilvitskii, S. k-means++: the advantages of careful seeding. in *Proceedings of the eighteenth annual ACM-SIAM symposium on Discrete algorithms* 1027–1035 (Society for Industrial and Applied Mathematics, USA, 2007).

39. Milios, D., Camoriano, R., Michiardi, P., Rosasco, L. & Filippone, M. Dirichlet-based Gaussian Processes for Large-scale Calibrated Classification. Preprint at https://doi.org/10.48550/arXiv.1805.10915 (2018).

40. Wood, K. *et al.* QUOKKA, the pinhole small-angle neutron scattering instrument at the OPAL Research Reactor, Australia: design, performance, operation and scientific highlights. *J. Appl. Crystallogr.* **51**, 294–314 (2018).

41. Kline, S. R. Reduction and analysis of SANS and USANS data using IGOR Pro. *J. Appl. Crystallogr.* **39**, 895–900 (2006).

42. Hamley, I. & Castelletto, V. Small-Angle Scattering of Block Copolymers. in *Soft Matter Characterization* (eds. Borsali, R. & Pecora, R.) 1021–1081 (Springer Netherlands, Dordrecht, 2008). doi:10.1007/978-1-4020-4465-6_20.

43. Chen, L.-T., Chen, C.-Y. & Chen, H.-L. FCC or HCP: The stable close-packed lattice of crystallographically equivalent spherical micelles in block copolymer/homopolymer blend. *Polymer* **169**, 131–137 (2019).

44. Marciel, A. B., Srivastava, S., Ting, J. M. & Tirrell, M. V. Chapter Eight - SAXS methods for investigating macromolecular and self-assembled polyelectrolyte complexes. in *Methods in Enzymology* (ed. Keating, C. D.) vol. 646 223–259 (Academic Press, 2021).

45. Combet, J. Polyelectrolytes and small angle scattering. *EPJ Web Conf.* **188**, 03001 (2018).